J|A|C|S COMMUNICATIONS

Published on Web 05/24/2010

Core/Shell Pd/FePt Nanoparticles as an Active and Durable Catalyst for the Oxygen Reduction Reaction

Vismadeb Mazumder,[†] Miaofang Chi,[‡] Karren L. More,[‡] and Shouheng Sun[†,*]

Department of Chemistry, Brown University, Providence, Rhode Island 02912, and Oak Ridge National Laboratory, Oak Ridge, Tennessee 37831

Received March 23, 2010; E-mail: ssun@brown.edu

The synthesis of active and durable catalysts for the oxygen reduction reaction (ORR) is one of the urgent needs in the development of fuel cell devices for practical applications. Numerous efforts have been devoted to the optimization of the existing platinum (Pt) nanoparticle (NP) catalysts[1] and to the design of new catalysts with less or no usage of Pt.[2] In addition to NP morphology control, recent research has also focused on fabrication of multicomponent metal catalysts to modify the Pt electronic structure and improve the Pt catalytic efficiency. Among the various multicomponent systems studied, Pt monolayers supported on Pd(111) film surfaces,[3] MPt alloy films (M = Fe, Co, Ni),[4] and FePt NPs[5] have attracted much attention. Although these catalysts are more active for ORR than their Pt counterparts and their enhanced activity is attributed to the strong interactions between Pt and other metals in the structure, the catalysts still lack the desired durability in the strong acidic medium of either $HClO_4$ or H_2SO_4 for ORR.

Here we report a unique approach for synthesizing core/shell-structured Pd/FePt NPs with a 5 nm Pd core and a FePt shell whose thickness is tunable from 1 to 3 nm. We demonstrate that the ORR catalysis of the Pd/FePt NPs is dependent on the FePt shell thickness and that the thin (1 nm or less) FePt shell is both active and durable for ORR in 0.1 M $HClO_4$ solution. These Pd/FePt NPs are a promising new catalyst candidate for practical fuel cell applications.

To make the core/shell Pd/FePt NPs, we first prepared 5 nm Pd NPs (Figure S1 in the Supporting Information) by the reduction of $Pd(acac)_2$ (acac = aceylacetonate) in the presence of oleylamine and borane *t*-butylamine at 75 °C.[6] We then coated these Pd NPs with FePt.[7] In a typical synthesis of 5 nm/1 nm Pd/FePt NPs, $Pt(acac)_2$ (0.15 mmol), oleylamine (6 mmol), and oleic acid (3 mmol) were mixed in 1-octadecene solvent (8 mL) and heated to 110 °C. The Pd seeding NPs (30 mg) in hexane (2 mL) were then added to the reaction mixture. Iron pentacarbonyl [$Fe(CO)_5$, 0.1 mL, 0.15 mmol] was injected into the reaction solution, which was then further heated to 180 °C. After the reaction mixture was cooled to room temperature, the product was separated and redispersed in 5 mL of hexane.[7]

The Pd/FePt NPs were characterized by transmission electron microscopy (TEM) and aberration-corrected high-angle annular dark-field scanning TEM (HAADF-STEM). While TEM gives the needed overall size and structural information of various core/shell NPs, it cannot distinguish the fine structural differences between Pd and Pt in the core/shell structure. Contrast variations in HAADF-STEM images are proportional to the square of the element's atomic number and can therefore provide key information regarding the elemental distribution within nanostructures at subangstrom resolution.[8] Figure 1A,B shows HAADF-STEM images of the 5 nm/1 nm Pd/FePt NPs. The high-resolution HAADF-STEM image shows darker contrast in the core and brighter contrast in the shell, indicating that the core contains lighter elements (Pd) than the shell

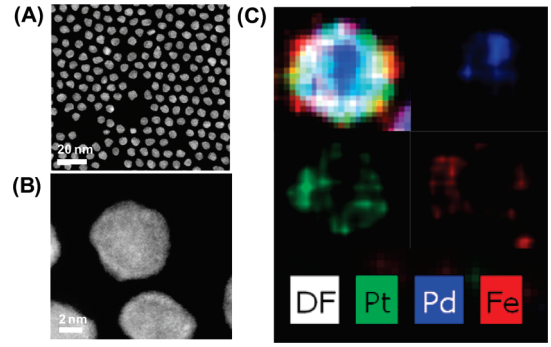

Figure 1. (A) HAADF-STEM, (B) high-resolution HAADF-STEM, and (C) elemental mapping images of the 5 nm/1 nm Pd/FePt NPs. The experiments were carried out on an aberration-corrected JEOL 2200FS microscope. HAADF-STEM images were acquired with a convergence angle of 27 mrad and an inner collection angle of 100 mrad. EDS analysis was carried out with an electron beam size of ~2 Å.

(Pt). The average core size and shell thickness were measured to be 4.9 ± 0.8 and 0.9 ± 0.1 nm, respectively, on the basis of measurements on 40 NPs. The compositional architecture of these core/shell NPs was further supported by high-resolution energy-dispersive spectroscopy (EDS) with an electron probe size of ~2 Å at angstrom-level resolution (Figure S2). A minimum of 18 individual NPs were compositionally analyzed, and the compositional distribution within each NP from the same sample was found to be consistent. Figure 1C displays the elemental mapping of a typical 5 nm/1 nm Pd/FePt NP. We can see that the NP contains Pt (green) and Fe (red) in the shell and Pd (blue) in the core. The FePt composition was further quantified by inductively coupled plasma−atomic emission spectroscopy (ICP−AES). The FePt shell in the 5 nm/1 nm Pd/FePt NPs has a composition of $Pd/Fe_{49}Pt_{51}$.

In the Pd/FePt synthesis, the FePt composition was controlled by the molar ratio of $Fe(CO)_5$ and $Pt(acac)_2$, and the FePt shell thickness was tuned by controlling the weight ratio of the Fe and Pt precursors and the Pd NP seeds. Under conditions similar to those for the synthesis of 5 nm/1 nm Pd/FePt NPs, 25 and 20 mg of Pd NP seeds resulted in Pd/FePt NPs with 2 nm $Fe_{40}Pt_{60}$ shells (Figure S3A) and 3 nm $Fe_{33}Pt_{67}$ shells (Figure S3B), respectively.

The presence of $Fe(CO)_5$ is an important factor that controls the uniform FePt coating on the Pd NPs. Without $Fe(CO)_5$, Pt did not nucleate on the Pd NP seeds. Rather, Pt NPs formed separately and precipitated from the reaction solution. It seems that under the current synthesis conditions, the decomposition of $Fe(CO)_5$ initiates nucleation and then facilitates the growth of FePt on the Pd NP surfaces. To control the FePt growth on Pd, the reaction temperature had to be kept below 200 °C and large amounts of $Fe(CO)_5$ had to be avoided. Higher temperatures or addition of more $Fe(CO)_5$ (for example, >0.5 mmol) promoted the separate nucleation of Fe components. The amount of Pd NP seeds also affects the FePt shell

[†] Brown University.
[‡] Oak Ridge National Laboratory.

10.1021/ja1024436

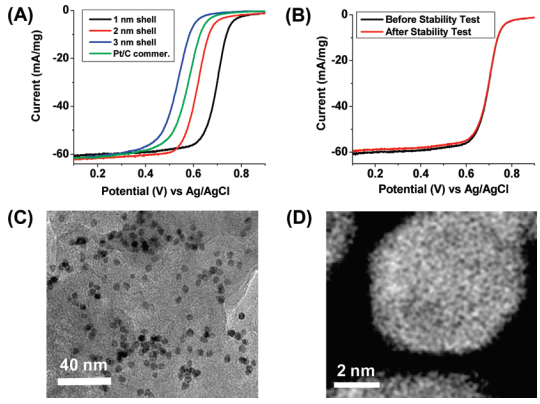

Figure 2. (A) Polarization curves showing the ORR current for three kinds of Pd/FePt NPs and the commercial 3.2 nm Pt NP catalyst. The current was normalized against the total mass of NPs used, and the electrode rotation rate was kept at 1600 rpm. (B) Comparative ORR activities of the 5 nm/1 nm Pd/FePt NPs before and after 10 000 potential cycles. (C) TEM image of the 5 nm/1 nm Pd/FePt NP/C catalyst after the ORR test and 10 000 potential cycles. (D) HAADF-STEM image of a typical 5 nm/1 nm Pd/FePt NP after 10 000 potential cycles.

formation. In the presence of 20−30 mg of Pd NPs, FePt nucleated and grew uniformly on the Pd seeds. More Pd NPs (e.g., 35 mg) led to multiple nucleations and the formation of both core/shell Pd/FePt NPs and Pt NPs. This could be avoided by using more (e.g., 70 mg) of Pt precursor. Under the current synthetic conditions, $Pt(acac)_2$/Pd NP weight ratios in the 3:1 to 2:1 range were critical for the formation of continuous FePt shells on the Pd NPs.

The controlled FePt coating over the Pd core offers the Pd/FePt NPs the much-desired structural and compositional tunability for ORR catalysis. To perform the catalytic tests, we first deposited the Pd/FePt NPs on a Ketjen carbon support via sonication of equal amounts of the two constituents in 5 mL of hexane and acetone, respectively.[7] The surfactant surrounding each NP was removed by an acetic acid (99%) wash at 70 °C.[7] During the acid wash, a significant portion of the Fe was lost, leaving only ∼5% Fe within the FePt shell in each of the Pd/FePt NPs with 1, 2, and 3 nm FePt coatings. However, Fe leaching did not affect the core/shell morphology of the Pd/Fe_5Pt_{95} NPs, as confirmed by HAADF-STEM images (Figure S4). Therefore, after this acid wash, we obtained three different kinds of Pd/Fe_5Pt_{95} NP catalysts among which the only variation was the FePt shell thickness.

The Pd/Fe_5Pt_{95}/C samples were redispersed in deionized water (2 mg/mL), and 20 μL of this dispersion was deposited on the glassy carbon surface of a rotating disk electrode (RDE) for ORR studies in O_2-saturated 0.1 M $HClO_4$ at 308 K.[7] The current generated from ORR was normalized by dividing the measured raw electrode currents by the mass of NPs (20 μg).[7] Figure 2A summarizes the observed current of the ORR for the three different kinds of Pd/FePt NPs and a commercial 3.2 nm Pt catalyst (BASF). We can see that at the half-wave potential (∼0.7 V), the current density generated from the 5 nm/1 nm Pd/FePt NPs was ∼12 times higher than that from the commercial Pt catalyst. More importantly, the Pd/FePt NPs with the 1 nm FePt coating were 15 times more active than those with the 3 nm coating and possessed a ∼140 mV more positive ORR onset potential. These results indicate that the ORR activity of the Pd/FePt NPs is dependent on the FePt shell thickness, with the thinner FePt shell having higher activity.

The 5 nm/1 nm Pd/FePt NPs were also stable under the ORR conditions. Durability tests were performed by cycling the potential between 0.4 and 0.9 V (vs Ag/AgCl) in O_2-saturated 0.1 M $HClO_4$. Figure 2B shows the ORR activities for the 5 nm/1 nm Pd/FePt NPs before and after 10 000 potential cycles. The overlapping $I-V$ curves indicate that the NPs had no obvious loss in surface area or activity after these potential cycles. TEM and HAADF-STEM analyses further confirmed that the 5 nm/1 nm Pd/FePt NPs had no noticeable change in morphology after the ORR test and 10 000 potential cycles and that the core/shell structure was maintained (Figure 2C,D).

The high activity of the 5 nm/1 nm Pd/FePt NPs may result from the electronic structure change of Pt upon its alloying with Fe.[4] However, since the NPs contained only 5% Fe and pure FePt NPs did not show such a drastic activity enhancement in ORR over the commercial Pt catalyst (Figure S5), we conclude that the alloying effect should not be a key factor in the enhancement. Rather, interfacial interactions between the thin FePt shell and the Pd core must dominate the ORR activity increase. The much-enhanced ORR stability of the 5 nm/1 nm Pd/Fe_5Pt_{95} NPs may also arise from the thin FePt coating, as a thin metallic shell can offer the desired thermodynamic stability for a metallic core/shell structure.[9] As a comparison, under similar test conditions, the Pd/FePt NPs with thicker FePt coatings and the commercial Pt catalyst showed poor stability with various NP aggregations (Figures S6 and S7). Detailed studies of the mechanisms that lead to the drastic activity and durability increase of these 5 nm/1 nm Pd/Fe_5Pt_{95} NPs are underway.

This communication has highlighted the unique synthesis of core/shell Pd/FePt NPs and their ORR catalysis. The uniform FePt shell was formed by controlled nucleation of $Fe(CO)_5$ in the presence of a Pt salt and Pd NPs at designated reaction temperatures. The Pd/FePt NPs showed FePt shell-dependent catalytic properties, and those having a 1 nm coating exhibited drastic increases in durability and activity (15 times more active with a 140 mV gain in onset potential in comparison with those having a 3 nm coating). The multimetallic core/shell NPs reported here have several distinct advantages over any of the previously reported NP systems: (1) the catalytically active shell is deposited uniformly on the core surface and is readily activated; (2) the shell thickness is controlled, and core/shell interactions can be tuned to optimize catalytic performance; and (3) the synthesis is versatile and allows different metals to be incorporated into either the core or the shell structure, offering a rich variety of core/shell NPs for catalytic applications.

Acknowledgment. This work was supported by the U.S. Department of Energy, Office of Energy Efficiency and Renewable Energy, Fuel Cell Technologies Program.

Supporting Information Available: Particle synthesis procedures, electrochemical studies, and other characterizations. This material is available free of charge via the Internet at http://pubs.acs.org.

References

(1) (a) Lee, H.; Habas, S. E.; Kweskin, S.; Butcher, D.; Somorjai, G. A.; Yang, P. *Angew. Chem., Int. Ed.* **2006**, *45*, 7824. (b) Ren, J.; Tilley, R. D. *J. Am. Chem. Soc.* **2007**, *129*, 3287. (c) Wang, C.; Daimon, H.; Onodera, T.; Koda, T.; Sun, S. *Angew. Chem., Int. Ed.* **2008**, *47*, 3588.
(2) (a) Lim, B.; Jiang, M.; Camargo, P. H.; Cho, E. C.; Tao, J.; Lu, X.; Zhu, Y.; Xia, Y. *Science* **2009**, *324*, 1302. (b) Peng, Z.; Yang, H. *J. Am. Chem. Soc.* **2009**, *131*, 7542. (c) Lefèvre, M.; Proietti, E.; Jaouen, F.; Dodelet, J.-P. *Science* **2009**, *324*, 71.
(3) (a) Zhang, J.; Vukmirovic, M. B.; Xu, Y.; Mavrikakis, M.; Adzic, R. R. *Angew. Chem., Int. Ed.* **2005**, *44*, 2132. (b) Zhou, W.; Yang, X.; Vukmirovic, M. B.; Koel, B. E.; Jiao, J.; Peng, G.; Mavrikakis, M.; Adzic, R. R. *J. Am. Chem. Soc.* **2009**, *131*, 12755. (c) Wang, J. X.; Inada, H.; Wu, L.; Zhu, Y.; Choi, Y.; Liu, P.; Zhou, W.-P.; Adzic, R. R. *J. Am. Chem. Soc.* **2009**, *141*, 17298.
(4) Stamenkovic, V. R.; Mun, B. S.; Arenz, M.; Mayrhofer, K.J. J.; Lucas, C. A.; Wang, G.; Ross, P. N.; Markovic, N. M. *Nat. Mater.* **2007**, *6*, 241.
(5) Kim, J.; Lee, Y.; Sun, S. *J. Am. Chem. Soc.* **2010**, *132*, 4996.
(6) Mazumder, V.; Sun, S. *J. Am. Chem. Soc.* **2009**, *131*, 4588.
(7) See the Supporting Information.
(8) (a) Kirkland, E. J.; Loane, R. F.; Silcox, J. *Ultramicroscopy* **1987**, *23*, 77. (b) Nellist, P. D.; Pennycock, S. J. *Ultramicroscopy* **1999**, *78*, 111.
(9) Paz-Borbon, L. O.; Mortimer-Jones, T. V.; Johnston, R. L.; Posada-Amarillas, A.; Barcaro, G.; Fortunelli, A. *Phys. Chem. Chem. Phys.* **2007**, *9*, 5202.

JA1024436